1

Covert cavitation: Spectral peak suppression in the acoustic emissions from spatially

configured nucleations

4

5

Jae Hee Song

Cavitation Laboratory (CavLab), Medical and Industrial Ultrasonics, School of Engineering,

University of Glasgow, Glasgow, G12 8QQ, United Kingdom

JaeHee.Song@glasgow.ac.uk

10

Kristoffer Johansen

Cavitation Laboratory (CavLab), Medical and Industrial Ultrasonics, School of Engineering,

University of Glasgow, Glasgow, G12 8QQ, United Kingdom

k.johansen.1@research.gla.ac.uk

15

Paul Prentice

Cavitation Laboratory (CavLab), Medical and Industrial Ultrasonics, School of Engineering,

University of Glasgow, Glasgow, G12 8QQ, United Kingdom

Paul.Prentice@glasgow.ac.uk

20

21

Running title: Covert cavitation

23

24 **Abstract**

25

26 Dual laser-nucleation is used to precisely configure two cavitation bubbles within a focused

27 ultrasound field of $f_0 = 692$ kHz, in proximity to the tip of a needle hydrophone. With both

28 bubbles responding in the $f_0/2$ sub-harmonic regime, confirmed via ultra-high speed

29 shadowgraphic imaging, an emission spectrum with no sub-harmonic content is demonstrated,

30 for an inter-bubble spacing $\approx \lambda_0$. A spectral model for periodic shock waves from multiple

31 nucleations demonstrates peak suppressions at $nf_0/2$ when applied to the experiment, via a

32 windowing effect in the frequency domain. Implications for single-element passive detection of

33 cavitation are discussed.

34

35

37

38

39

41

42

43

44

45

47 **1. Introduction**

48

49 The emission of sub-harmonic signals from a medium during exposure to intense ultrasound, is

50 held to be exclusive to the presence of acoustic cavitation-bubble activity within that medium.

51 Indeed, detection at the sub-harmonics, particularly $f_0/2$ and higher-harmonics at $nf_0/2$, where f_0 is

52 the frequency of the acoustic driving, is regularly used to determine the onset of cavitation-

53 mediated effects in medical[1, 2] and industrial applications.[3, 4] Broadband emissions, which can

54 assessed between spectral peaks,[5] or over frequencies sufficiently greater than f_0,[6] is also

55 commonly used as an indicator for inertial cavitation.

56 We recently reported optical imaging and acoustic detection of single stable-inertial

57 cavitation events at high temporal resolution,[7] initiated via the laser-nucleation technique[8] and

58 driven by high-intensity focused ultrasound (HIFU). Shadowgraphic imaging facilitated via

59 synchronous pulsed-laser illumination, revealed periodic shock waves (PSWs) emitted at f_0/m

60 (where m is an integer value) from the bubble activity, dependent on the pressure amplitude of the

61 driving. Detector deconvolution from the acoustic data allowed reconstruction of the PSWs, and

62 their contribution to the cavitation spectrum to be quantitatively analyzed, validating a spectral

63 model that suggested PSWs generate features at nf_0/m, for all values of n and m (where n is an

64 integer value). The results indicated that PSWs were predominantly responsible for all features of

65 the cavitation noise spectrum, other than ~15 dB at f_0, attributable to linear scattering of the driving

66 field.

67 In this Letter, we describe an extension to the experimental capability such that two

68 acoustic cavitation events can be simultaneously nucleated, in predetermined spatial

69 configurations relative to each other, the tip of a needle hydrophone and HIFU focus. We present

70 ultra-high speed shadowgraphic imaging to confirm that both resulting cavitation-bubbles are

71 responding in the $f_0/2$ regime, yet the spectrum of the combined acoustic emissions reveals no

72 perceptible sub-harmonic content, or higher harmonics of the sub-harmonic. The spectral model

73 for PSWs is extended to account for a multi-nucleated system.

74

75 **2. Experimental arrangement**

76

77
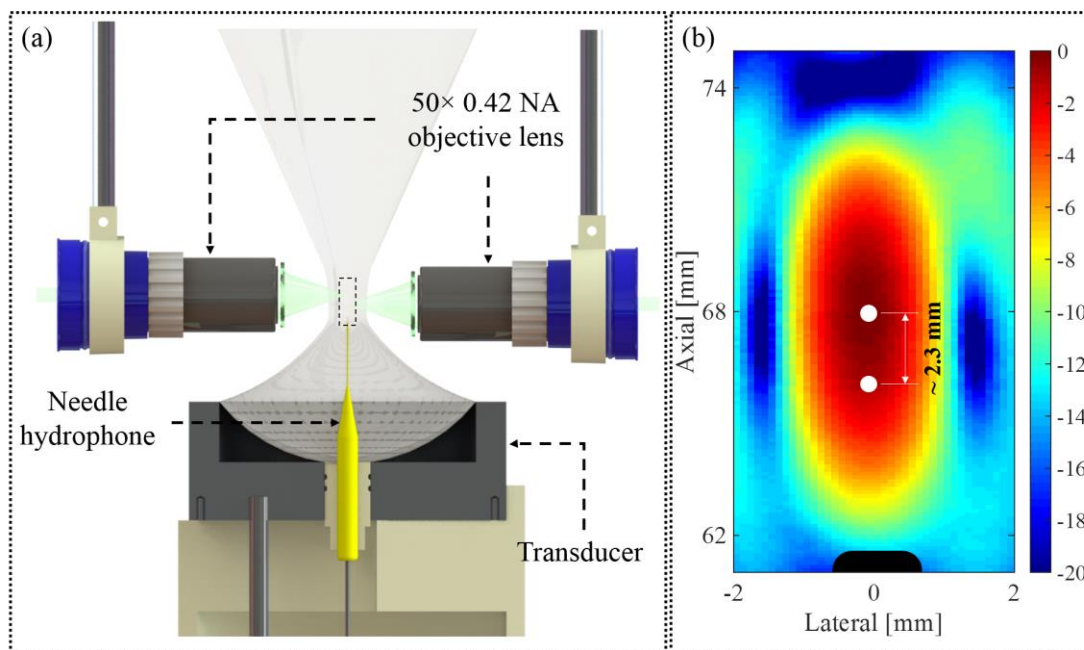
78

79

80   Fig. 1. (Color online) Illustration of experimental setup: (a) cross-sectional view of HIFU

81   transducer-NH configuration, and two long-working distance objective lenses facilitating dual-

82   laser nucleation of cavitation bubbles. (b) An axial scan of the HIFU focal region, including the

83   targeted laser-nucleation zones, to which the nucleating laser foci were aligned.

84   The experimental arrangement is broadly similar to that described in detail in our previous

85   report,[7] with two modifications distinguishing the current work. Briefly, a single element

86   piezoceramic transducer (H-149, Sonic Concepts, Bothell, WA), generates a 90-cycle burst of

87   HIFU at f_0 = 692 kHz and peak-positive pressure amplitude, $PPPA_{HIFU} \cong 1.63 \pm 0.12$ MPa, which

88   drives cavitation at the focus in the $f_0/2$ regime.[7] A needle hydrophone (NH, 1.0 mm diameter,

89   PVdF, Precision Acoustics, Dorchester, UK), calibrated for magnitude and phase over a bandwidth

90   of 125 kHz to 20 MHz, in 25 kHz increments[9] (National Physical Laboratory, Teddington, UK,

91   2016), is mounted within a central hole through the body of the HIFU transducer, such that it aligns

92   to the propagation axis of the field generated, Fig. 1 (a) and (b). Steps taken to measure the HIFU

93   amplitude with the NH in the inverted position, Fig. 1 (a), which may be expected to perturb the

94   field are described in detail.[7]

95   Cavitation is introduced to the focus of the HIFU field via the laser-nucleation technique.[8]

96   To generate the results presented below, however, a 50:50 beam splitter (BS010, Thorlabs, Ely,

97   UK) is introduced to the nucleating laser-pulse beam path. The component beams from a 2.4 ± 0.2

98   mJ (instrument error according to manufacturer), 6–8 ns laser pulse (Nano S 130-10 frequency

99   doubled Q-switched Nd:YAG, Litron Lasers, Rugby, UK), are steered to the back apertures of two

100   long-working distance microscope objective lenses (50× 0.42 NA Mitutoyo, Kawasaki, Japan),

101   Fig. 1 (a), sealed in water-tight units and mounted on xyz manipulators. This configuration permits

102   simultaneous dual laser-nucleation of two, independently positioned, cavitation-bubbles, Fig. 2.

103   Ultra-high speed imaging is undertaken at 5×10^6 frames per second (fps) with a Shimadzu

104   HPV-X2 camera (Shimadzu, Kyoto, Japan), with 256 frames per sequence. Synchronous 10 ns

105   laser pulses (CAVILUX Smart, Cavitar, Tampere, Finland) provide the illumination and effective

106   temporal resolution, per frame. A macro-objective lens (Zeiss 100mm f2 Makro-Planar Milvus

107 ZF.2, Oberkochen, Germany) facilitates a larger field of view than that reported previously,[7] such

108 that HIFU propagation as well as shock wave emission from cavitating bubbles, can be

109 visualized.[10]

110

111 **3. Results**

112

113 *3.1 High-speed imaging*

114

115 Figure 2 depicts representative images extracted from a high-speed sequence of dual-nucleated

116 acoustic cavitation activity, each comparable to the single bubble $f_0/2$ regime activity reported

117 previously,[7] characterized by stable $f_0/2$ PSW emission. At the field of view delivered by the

118 macro-objective, the bubble activity is barely resolved. However, the compressional and

119 rarefactional phases of the propagating HIFU can be appreciated,[10] as fringes slightly brighter and

120 darker than the ambient background (labelled C and R, Figure 2), respectively. The effect is better

121 perceived from the movie version of the data, Mm.1, where it can also be seen that the bubbles

122 collapse and emit shockwaves in response to every other compressional phase, confirming the $f_0/2$

123 response regime. The salient features of this data are two cavitating bubbles (hereafter referred to

124 as top^t and bottom^b bubbles), separated by 2.3 ± 0.1 mm, which compares to the HIFU wavelength,

125 $\lambda_0 = 2.14$ mm, emitting $f_0/2$ PSWs approximately in-phase. Intuitively, this leads to a combined

126 effective shock wave detection frequency of f_0, at the NH tip, visible to the bottom of each image,

127 Fig. 2.

128

129
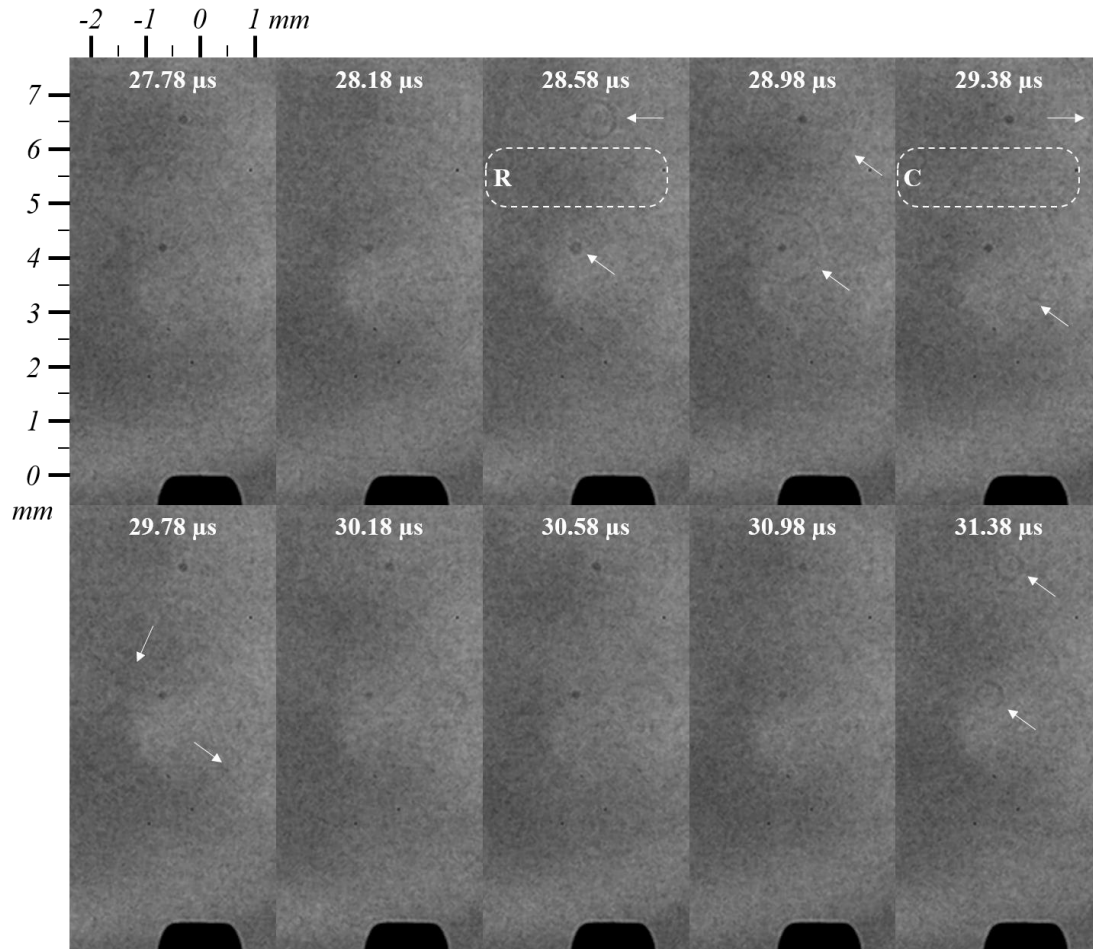
Fig. 2. Selected high-speed shadowgraphic images from Mm. 1, recorded at 5×10^6 fps, of two cavitation-bubbles with an inter-bubble spacing $\approx \lambda_0$. Transitory brighter and darker regions, imposed over an already inhomogeneous background illumination, such as indicated by dash box C and R, represent compressional and rarefactional phases of the HIFU driving. The propagating HIFU can be better perceived in the movie version of the data Mm. 1. PSW emission, arrowed at 28.58 µs and 31.38 µs (but not 30.18 µs, when an intervening compressive phase is incident) verifies that both bubbles are in the $f_0/2$ sub-harmonic regime.

140   Mm. 1. Movie of the entire image sequence represented in Fig. 2, at full field of

141   view, showing in phase $f_0/2$ PSW emission from both bubbles. Video duration is

142   20s, file type "avi" (1.74 MB).

143

144 *3.2 Hydrophone data*

145

146 Figures 3 (a) and (b) (solid grey) represent the needle hydrophone data collected during the

147 cavitation activity represented in Fig. 2, deconvolved from the impulse response of the hydrophone

148 with magnitude and phase calibration. A HIFU control exposure, for which a burst of identical

149 parameters was generated, but no cavitation nucleated, has also been subtracted.

150   A synthetic PSW signal (red dot, Figs. 3 (a) and (b)), is constructed from simulated shock

151 wave profiles, derived from solving the Gilmore equation for a freely collapsing resonant bubble,

152 and fitted to the experimental data.[7] Synthetic acoustic f_0 and $2f_0$ components from both bubbles

153 in combination, of amplitudes and phases 10.68 ± 0.62 kPa, $121.75° \pm 5.31°$ and 1.88 ± 0.52 kPa

154 and $52.59° \pm 21.96°$, respectively, can be added for consistency with the full synthetic spectrum

155 construction procedure described previously.[7] This yields a cross correlation coefficient of 0.96

156 between the full synthetic and experimental spectra (solid grey, Fig. 3 (c)), indicating the signal is

157 well represented. However, for the purpose of developing the model below to derive a window

158 function in the frequency domain, we consider only the PSW spectra (red dot, Fig 3. (c)) of the

159 synthetic PSW signal, which presents peaks at all relevant frequency values.

160   Inspection of the PSW profiles of Fig. 3 (b), demonstrates that the shock waves from the

161 top and bottom bubbles can be distinguished by their full-width at half maximum (FWHM), with

162 the wider shocks from the lower bubble, detected at 31.66 and 34.37 µs, due to the more oblique

163 incidence to the NH tip. Bandpass filtering of the experimental deconvolved and control-subtracted

164 NH signal, Fig. 3 (a), from 1.5 to 20 MHz to remove f_0 and $2f_0$ components within the NH

165 calibration range, reveals detected shock widths of $FWHM_{PSW}^{t} = 40.57 \pm 3.97$ and $FWHM_{PSW}^{b} =$

166 65.00 ± 7.62 ns from the top and bottom bubbles, respectively.

167
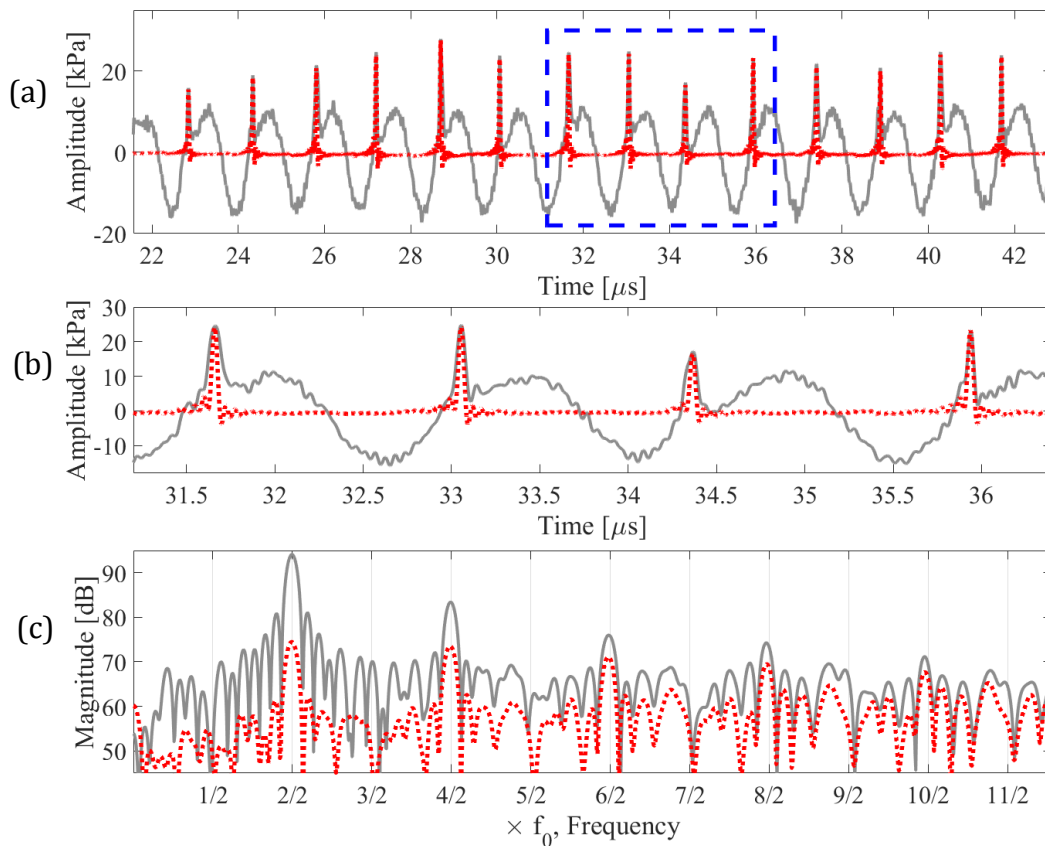
168

169 Fig. 3. (Color online) (a) Pressure-time waveforms of control-subtracted and deconvolved NH

170 data (solid grey) and synthetic PSW signal (red dot), with the blue-dash box reproduced in (b)

171 corresponding directly to the selected images of Fig. 2. (c) The experimental NH (solid grey) and

172 PSW synthetic (red dot) spectra for the combination system, revealing no sub-harmonic content

173 including at odd-numbered higher harmonics.

174

175   Analysis of Fig. 3 (a) also reveals that the period of shock wave emission, $T_{PSW}^t = 2.893 \pm$

176   0.068 µs and $T_{PSW}^b = 2.905 \pm 0.116$ µs, compared to $2T_0 = 2.890$ µs, for the HIFU field.

177

178   **4.   Spectral analysis model for dual bubbles**

179

180   To analyze the effect on the spectrum of the combined emissions from the dual cavitation-bubble

181   system represented in Fig. 2, we consider the synthetic PSW signal that would be detected by the

182   NH from both bubbles, $x_{PSW}^{NH}(t)$, as the sum of the synthetic PSW signals from the top bubble,

183     $x_{PSW}^t(t)$, and bottom bubble, $x_{PSW}^b(t)$, emitted in isolation from the other. The effects of bubble-

184   bubble interactions, which will be particularly prevalent at smaller inter-bubble distances, are

185   discussed below. $x_{PSW}^t(t)$ and $x_{PSW}^b(t)$ are deduced from the distinct shock wave profile FWHMs

186   apparent from Fig. 3 (b), in combination with the high speed image sequence of the activity, such

187   that each shock wave and its source bubble is individually identified. As both bubbles are

188   responding to the HIFU in the same $f_0/2$ sub-harmonic regime, $x_{PSW}^t(t)$ can be approximated in

189   terms of $x_{PSW}^b(t)$, as

190     $$x_{PSW}^t(t) \approx r \cdot x_{PSW}^b(t - \tau) \tag{1}$$

191

192   where r is the ratio of peak-positive pressure amplitudes $PPPA_{SW}^t : PPPA_{SW}^b$, of the PSWs from

193   the top and bottom bubbles, respectively, and τ is the difference in propagation time from each

194   bubble, to the NH tip. The frequency spectrum of the combined PSW signal detected by the NH,

195     $X_{PSW}^{NH}(f) = \mathcal{FT}\{x_{PSW}^{NH}(t)\}$, where $\mathcal{FT}\{\cdot\}$ is the Fourier transform, can therefore be expressed in

196   terms of the magnitude of the PSW spectrum from the bottom bubble, as

197
$$|X_{PSW}^{NH}(f)| \approx |1 + r \cdot cos(2\pi f \tau)| \cdot |X_{PSW}^{b}(f)| \tag{2}$$

198

199   The $[1 + r \cdot cos(2\pi f \tau)]$ term of Eq. (2) acts as a "periodic windowing" function to the

200   magnitude response of the PSW spectrum of the bottom cloud, to obtain magnitude of the NH

201   spectrum, $|X_{PSW}^{NH}(f)|$. τ thus determines the spacing of the window suppressions in the frequency

202   domain, with r determining the degree of suppression. To apply the model to the dual-bubble

203   cavitation system of Fig. 2, values are ascertained for the windowing parameters as $\tau = 1.444 \pm$

204     $0.074 \, \mu s$, and r $= 1.07 \pm 0.18$ (with $PPPA_{SW}^{t} = 22.92 \pm 2.20 \, kPa$ and $PPPA_{SW}^{b} = 21.91 \pm 4.29 \, kPa$).

205   The resulting window function (solid blue, Fig. 4) imposed to the synthetic PSW spectrum,

206     $X_{PSW}^{b}(f)$ (red dot), of the bottom bubble, generates the PSW spectrum as detected by the NH from

207   the dual-bubble system, $X_{PSW}^{NH}(f)$ (solid red).

208
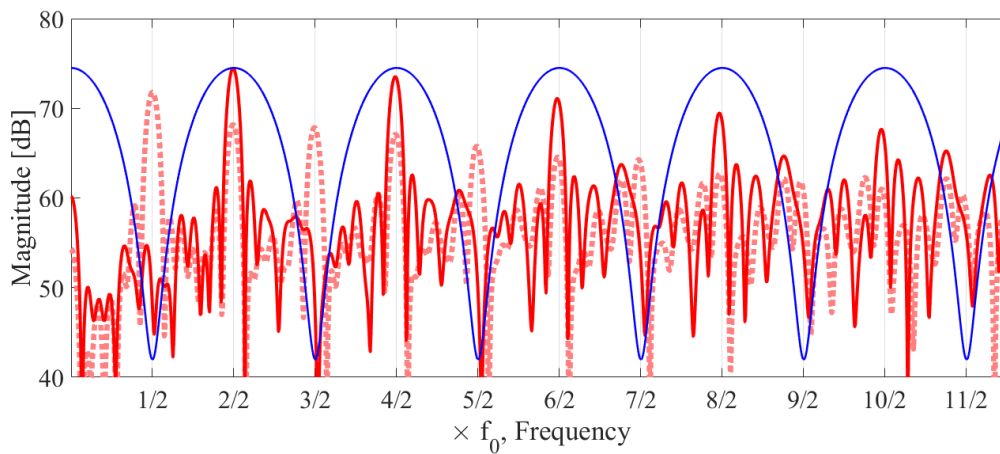
209

210   Fig. 4. (Color online) The magnitude of the synthetic $f_0/2$ PSW spectrum, $|X_{PSW}^{b}(f)|$, expected

211   from the bottom bubble only (red dot), the windowing function (solid blue) with r and τ deduced

212   from the experimental NH data, and the resulting NH PSW spectrum, $|X_{PSW}^{NH}(f)|$ (solid red), on

213   application of the window.

214   Figure 4 confirms that $X_{PSW}^b(f)$, in isolation, generates peaks at all values of $nf_0/2$,

215   including the sub-harmonic and its higher harmonics, and f_0 and its higher harmonics, consistent

216   with our previous report.[7] In applying the window function of Eq. (2), to deduce the PSW spectrum

217   from the dual-bubble system, however, all spectral content at $nf_0/2$ for odd-values of n, are

218   suppressed, in line with the experimental spectrum of the dual-bubble emissions, collected by the

219   NH, (solid grey, Fig. 3 (c)).

220

221   **5. Discussion**

222

223   With this experiment, we have definitively demonstrated that a medium can host cavitation activity,

224   of a particular regime, and yet appear not to generate the acoustic signals specifically associated

225   with that regime. In the particular example presented, the cavitation sub-harmonic at $f_0/2$, and its

226   higher harmonics, which are signals widely used to infer the very existence of acoustic cavitation,[1-

227   4] are significantly suppressed for any detector aligned to the HIFU axis. A windowing function is

228   analytically expressed to predict the frequency values at which peak suppressions will occur for

229   the spectrum of the dual-bubble cavitation activity, in terms of the PSW spectrum from one of the

230   component bubbles. This confirms suppression at $nf_0/2$, for odd values of n, as seen in the

231   experimental results. Moreover, the resulting signal enhancement, at even values of n (harmonics

232   of f_0), could easily be misinterpreted as due to nonlinear HIFU propagation, rather than cavitation

233   activity.

234   From Fig. 2, the distance between the hydrophone tip and the top and bottom bubbles is

235   6.6 and 4.3 ± 0.1 mm, respectively. Fig. 3 (b) indicates that the maximum instantaneous amplitude

236   of the emissions from each bubble ≈ 30 kPa. Assuming the pressure amplitude decays in inverse

237   proportion to the propagation distance, the highest instantaneous pressure within the emissions

238   from the source bubble, at the location of the second bubble, is ~ 100 kPa. The analysis therefore

239   assumes that the emissions from either bubble are dominated by the HIFU driving, and not

240   significantly influenced by the other bubble, for the short duration of ~ 20 µs over which they are

241   sampled. For extended driving durations, and smaller inter-bubble distances, bubble-bubble

242   interactions will become significant. For example, secondary radiation force-induced translation,

243   which is not perceptible within the high speed imaging of Fig. 2 and Mm. 1, would lead to

244   windowing parameters that are also a function of time.

245   The model easily allows other configurations of two $f_0/2$ bubbles to be considered, under

246   the assumption that they can be considered as two independent sources. If the bubbles, emitting

247   PSWs in phase, were configured orthogonally to the HIFU propagation axis, at an inter-bubble

248   spacing of λ_0, the shock waves from each bubble would arrive at the hydrophone tip, at the same

249   time. The magnitude of the $f_0/2$ peak would therefore be double that from either bubble, emitting

250   individually. Alternatively, an inter-bubble spacing of $\lambda_0/2$, along the HIFU propagation axis, will

251   result in an effective shock wave detection frequency of $2f_0$ at the hydrophone. This would halve

252   the value of τ used above, doubling the frequency values at which suppression occurs, such that

253   odd-order f_0 harmonics (f_0, $3f_0$, $5f_0$, $7f_0$…) are suppressed.

254   More than two bubbles responding in the same regime would result in additional r and τ

255   values, and more complex periodic windowing functions, of variable frequency spacing and

256   degrees of suppression. For multiple cavitation-bubbles responding to an insonation in different

257   sub-harmonic regimes, such as for a HIFU field with bubbles simultaneously within the focus and

258   also outside of it, the windowing function cannot be analytically derived. However, the presented

259   model may be applicable for combinations of f_0/n and f_0/m (where $n \neq m$) bubbles within limited

260   frequencies, if they have common spectral peaks at $k \cdot L \cdot f_0$ where $k \in \mathbb{N}$, and L is the least common

261   multiple of $1/m$ and $1/n$. By taking the approximation that $X_{PSW}^b(f) \approx r' \cdot X_{PSW}^t(f)$ where $r' =$

262    $r \cdot m/n$ and $f = k \cdot L \cdot f_0$, constructive and destructive interference at specific spectral peaks may be

263   anticipated.

264   Evidently, the precision of laser-nucleation has allowed us to spatially configure bubble

265   activity for maximum effect, to demonstrate spectral windowing and peak suppression. The near-

266   complete suppression, demonstrated here for $f_0/2$ because the shock wave amplitude ratio, $r \approx 1$,

267   of any peak would not be expected for experiments involving spontaneous and stochastically

268   distributed cavitation. We also note that the experimental results presented above have been

269   selected from a longer data set, as an ideal case in terms of shock wave amplitude and periodicity,

270   to demonstrate the effect. Generally, however, care should be taken with gauging the level of

271   cavitation activity from the magnitude of any single spectral peak.

272   A second detector, aligned orthogonally to the one in the configuration described here,

273   would certainly be expected to detect sub-harmonic signal. This would indicate that multiple,

274   spatially configured cavitation detectors would yield reliable, and reproducible measurements for

275   correlation of cavitation-mediated effects, particularly for systems where a low number of

276   nucleations may be anticipated. Parallel assessment of cavitation emissions over a sufficiently

277   large bandwidth will also minimize the effects of spectral windowing.

278

279   **Acknowledgements**

280

14

283   Grant Agreement no. 336189 (TheraCav). The authors acknowledge Miriam Jiménez García for

284   technical assistance.

285

286   **References**

287

288   [1]C. M. Schoellhammer, A. Schroeder, R. Maa, G. Y. Lauwers, A. Swiston, M. Zervas, R.

289   Barman, A. M. DiCiccio, W. R. Brugge, D. G. Anderson, D. Blankschtein, R. Langer, and G.

290   Traverso, "Ultrasound-mediated gastrointestinal drug delivery," Sci. Transl. Med. **7**, 310ra168

291   (2015).

292   [2]M. A. O'Reilly and K. Hynynen, "Blood-Brain Barrier: Real-time feedback-controlled focused

293   ultrasound disruption by using an acoustic emission-based controller," Radiology **263**, 96-106

294   (2012).

295   [3]K. Kawabata and S. Umemura, "Use of second-harmonic superimposition to induce chemical

296   effects of ultrasound," J. Phys. Chem., **100**, 18784-18789 (1996).

297   [4]H. Hasanzadeh, M. Mokhtari-Dizaji, S. Z. Bathaie, and Z. M. Hassan, "Evaluation of

298   correlation between chemical dosimetry and subharmonic spectrum analysis to examine the

299   acoustic cavitation," Ultrason. Sonochem., **17**, 863-869 (2010).

300   [5]W. S. Chen, A. A. Brayman, T. J. Matula, and L. A. Crum, "Inertial cavitation dose and

301   hemolysis produced *in vitro* with or without Optison," Ultrasound Med. Biol., **29**, 725-737

302   (2003).

303   [6]C. C. Coussios, C. H. Farny, G. ter Haar, and R. A. Roy, "Role of acoustic cavitation in the

304   delivery and monitoring of cancer treatment by high-intensity focused ultrasound (HIFU)," Int. J.

305   Hyperthermia, **23**, 105-120 (2007).

306   [7]J. H. Song, K. Johansen, and P. Prentice, "An analysis of the acoustic cavitation noise spectrum:

307   The role of periodic shock waves," J. Acoust. Soc. Am., **140**, 2494-2505 (2016).

308   [8]B. Gerold, S. Kotopoulis, C. McDougall, D. McGloin, M. Postema, and P. Prentice, "Laser-

309   nucleated acoustic cavitation in focused ultrasound," Rev. Sci. Inst. **82**, 044902 (2011).

310   [9]K. Johansen, J. H. Song, K. Johnston, and P. Prentice, "Deconvolution of acoustically detected

311   bubble-collapse shock waves," Ultrasonics, **73**, 144-153 (2017).

312   [10]K. Johansen, J. H. Song, and P. Prentice, "Characterising focused ultrasound via high speed

313   shadowgraphic imaging at 10 million frames per second" IEEE Ultrasonics Symposium, Tours

314   (2016), pp. 1-4.

315

316

317